



# The CO anthropogenic emissions in Europe from 2011 to 2021: insights from the MOPITT satellite data.

Audrey Fortems-Cheiney<sup>1,\*</sup>, Gregoire Broquet<sup>1</sup>, Elise Potier<sup>1,\*\*</sup>, Robin Plauchu<sup>1</sup>, Antoine Berchet<sup>1</sup>, Isabelle Pison<sup>1</sup>, Hugo Denier van der Gon<sup>2</sup>, and Stijn Dellaert<sup>2</sup>

<sup>1</sup>Laboratoire des Sciences du Climat et de l'Environnement, CEA-CNRS-UVSQ, Gif-sur-Yvette, France

<sup>2</sup>Department of Climate, Air and Sustainability, TNO, P.O. Box 80015, 3508 TA Utrecht, Netherlands

\* now in Science Partners, Quai de Jemmapes, 75010 Paris, France

\*\* now in Laboratoire Inter-universitaire des Sciences Atmosphériques, Univ Paris Est Créteil and Université Paris Cité, CNRS, LISA, 94010 Créteil, France

**Correspondence:** Audrey Fortems-Cheiney, [audrey.fortems@science-partners.com](mailto:audrey.fortems@science-partners.com)

**Abstract.** We have used the variational inversion drivers of the recent Community Inversion Framework (CIF), coupled to a European configuration of the CHIMERE regional chemistry transport model and its adjoint to derive carbon monoxide (CO) emissions from the MOPITT TIR-NIR observations, for a period of over 10 years from 2011 to 2021. The analysis of the inversion results reveals the challenges associated with the inversion of CO emissions at the regional scale over Europe. Annual budgets of the national emissions are decreased by about 1-11% over the decade and across Europe. These decreases are mainly due to negative corrections during autumn and winter. The posterior CO emissions follow a decreasing trend over the European Union + United Kingdom area with a trend of about -2.2 %/year, slightly lower than in the prior emissions. The assimilation of the MOPITT observation in the inversions indeed attenuates the decreasing trend of the CO emissions in the TNO inventory over areas benefiting from the highest number of MOPITT super-observations (particularly over Italy and over the Balkans), and particularly in autumn and winter. The small corrections of the CO emissions at national scales by the inversion can be attributed, first, to the general consistency between the TNO-GHGco-v3 inventory and the satellite data. Analysis of specific patterns such as the impact of the covid-19 crisis reveal that it can also be seen as a lack of observation constraint to adjust the prior estimate of the emissions.



The large errors in the observations, and the lack of data over large parts of Europe are sources of limitation on the observational constraint. Emission hot spots generate a relatively strong local signal, which is much better caught and exploited by the inversions than the larger scale signals, despite the moderate spatial resolution of the MOPITT data. This is why the corrections of these hot spot emissions are stronger and more convincing than the corrections of the national and continental scale emissions. Accurate monitoring of the CO national anthropogenic emissions may thus require modeling and inversion systems at spatial resolution finer than those used here, as well satellite images at high spatial resolution. The CO data of the TROPOMI instrument onboard the Sentinel-5P mission should be well suited for such a perspective.

## Plain Language Summary

### 1 Introduction

Carbon monoxide (CO) is an air pollutant and a greenhouse gas, mainly emitted by anthropogenic activities, and impacting both the air quality and climate change. It has a major role in atmospheric chemistry, as a key component of the methane (CH<sub>4</sub>) oxidation chain with formaldehyde (HCHO), ozone (O<sub>3</sub>), and carbon dioxide (CO<sub>2</sub>). Through chemical interactions with hydroxyl radical (OH), CO i) influences concentrations of CH<sub>4</sub> and non-methane volatile organic compounds (NMVOCs), ii) affects the self-cleaning or oxidation capacity of the atmosphere (Lelieveld et al., 2016) and iii) leads to the chemical production of air pollutants and/or greenhouse gases such as tropospheric O<sub>3</sub> and CO<sub>2</sub>. In this context, there is a need for an accurate mapping/monitoring of the CO surface emissions.

CO emissions estimated by bottom-up (BU) inventories, based on statistical and economic data and relying on emission factors per activity type, suffer from relatively large uncertainties. For example, at the national and annual scales, these uncertainties range from 20-60% to 50-200% depending on the sectors in the European Monitoring and Evaluation Programme (EMEP) inventory (Kuenen and Dore, 2019). Complementary to BU inventories, atmospheric CO concentration data, such as those observed from satellite observations, can be used to derive estimates of the CO fluxes, based on atmospheric transport inverse modeling techniques (Rayner et al., 2019). Over the last two decades, the space-borne Measurement of Pollution in the Troposphere (MOPITT, Drummond et al., 1996; Deeter et al., 2003), the Atmospheric Infrared Sounder (AIRS, (Au-



mann et al., 2003; McMillan et al., 2005), Tropospheric Emissions Spectrometer (TES, (Beer, 2006) and Interféromètre Atmosphérique de Sondage dans l’Infrarouge (IASI, (Clerbaux et al., 2009)) have revolutionized our ability to map CO concentrations and to understand the trends of its concentrations and emissions (Fortems-Cheiney et al., 2011; George et al., 2015; Yin et al., 2015; Zheng et al., 2018; Buchholz et al., 2021). However, the potential of satellite data to inform about CO emissions has been mainly explored at the global scale, with emission estimates corresponding to large regions. Today, the scientific and societal issues require an up-to-date quantification of pollutant emissions at a higher spatial resolution, targeting national estimates. This currently requires the use of regional scale inversion systems (Fortems-Cheiney et al., 2021). However, although these systems are suited to reactive species, they have hardly been used to quantify emissions of pollutants such as CO. Konovalov et al. (2016) estimated CO European emissions from the IASI thermal-infrared (TIR) satellite measurements and pointed out the low sensitivity of the corresponding CO total columns to anthropogenic CO emissions over Europe. (Deeter et al., 2013) have shown that the sensitivity of total columns to CO emissions in the lower troposphere - where the regional signal from CO regional anthropogenic emissions above the large scale and highly mixed CO background is the largest - should be significantly greater for retrievals exploiting simultaneous TIR and near-infrared (NIR) measurements than for retrievals based on either spectral region alone. Fortems-Cheiney et al. (2021) have performed regional inversions using MOPITT TIR-NIR satellite observations over Europe to illustrate the behavior of the variational atmospheric inversion system PYVAR-CHIMERE, but only over a short temporal window of seven days. The ability of regional inverse systems to quantify CO budgets at the national scale from the MOPITT TIR-NIR satellite observations has not been assessed yet.

The objective of this work is therefore to carry out a long-term regional inversion for Europe using these observations. We estimate CO emissions from the MOPITT TIR-NIR observations, for more than 10 years from January 2011 to November 2021. The analysis over the period 2011-2021 makes it possible to evaluate the strong trends indicated by the BU inventories over the decade, and major inter-annual anomalies, in particular the expected reduction of emissions in 2020 due to the measures taken in response to the COVID-19 pandemic. For this objective, we have used the variational inversion drivers of the recent Community Inversion Framework (CIF, (Berchet et al., 2021)), which inherits the developments made for the regional assimilation of satellite data on gaseous species by Fortems-Cheiney et al. (2021). We also use a European configuration of the



CHIMERE regional chemistry transport model (CTM) (Menut et al., 2013; Mailler et al., 2017) and of its adjoint (Fortems-Cheiney et al., 2021), driven by the CIF. The data and methods used in this study are described in Section 2. The results are described in Section 3.

## 80 2 Data and Methods

### 2.1 Configuration of the CHIMERE CTM for the simulation of CO concentrations in Europe

The configuration of the atmospheric CTM CHIMERE for Europe is described in Table 1. CHIMERE is run over a  $0.5^\circ \times 0.5^\circ$  regular horizontal grid and 17 vertical layers, from the surface to 200hPa, with 8 layers within the first two kilometers. The domain covers Europe ( $15.25^\circ\text{W}$ - $35.75^\circ\text{E}$ ;  $31.75^\circ\text{N}$ - $74.25^\circ\text{N}$ ) and includes 101 (longitude)  $\times$  85 (latitude) grid-cells. The reanalyzes ERA-Interim – the only ones available at the beginning of this study - remain at the rather low horizontal resolution of 79 km compared to the forecast fields. Consequently, as a trade-off between accuracy of large-scale meteorological fields and resolution at finer resolution, CHIMERE is driven here by the European Centre for Medium-Range Weather Forecasts (ECMWF) operational meteorological forecast (Owens and Hewson, 2018), with a spatial resolution of  $0.25^\circ$ . The chemical scheme used in PYVAR-CHIMERE is MELCHIOR-2, with more than 100 reactions (CHIMERE, 2017), including the secondary production of CO through the oxidation and photolysis of hydrocarbons and its sink with OH.

Initial and boundary conditions for several key gaseous species responsible for the oxidation capacity of the lower atmosphere (e.g., CO, NO, NO<sub>2</sub>, O<sub>3</sub>, H<sub>2</sub>O<sub>2</sub>, HCHO, etc) were specified using monthly climatological data from LMDz-INCA global model (Szopa, 2008).

CO emissions from fires, that count for about 2% of the European total COemissions (San-Miguel-Ayanz and Steinbrecher, 2019), are not taken into account in this study. CO biogenic emissions are assumed to be negligible and are not taken into account. The prior estimate of CO anthropogenic emissions is derived from the recent TNO-GHGco-v3 gridded inventory for the period 2005-2018. The TNO-GHGco version is an update of the TNO inventory (Super et al., 2020; Denier van der Gon et al., 2021; Kuenen et al., 2022) based on EMEP/CEIP official country reporting for air pollutants. This inventory has been delivered with an extrapolation of the emissions for the year 2019, based on an in-sample approach (Super et al., 2020). We use this combination



Domain	Europe (15.25°W-35.75°E; 31.75°N-74.25°N)
Horizontal resolution	0.5°×0.5° regular grid
Vertical resolution	17 layers, from the surface to 200hPa
Meteorological fields	ECMWF operational meteorological forecast (Owens and Hewson, 2018)
Initial and boundary conditions	Climatological values from the LMDZ-INCA global model (Szopa, 2008)
Anthropogenic emissions	TNO-GHGco-v3 inventory (Super et al., 2020)
Biogenic emissions	MEGAN (Guenther et al., 2006)

**Table 1.** Main characteristics of the European CHIMERE configuration used in this work.

of products for the years 2005-2019. Our prior estimates of the emissions for 2020 and 2021 are set at the values for 2019. The horizontal resolution of the TNO-GHGco-v3 inventory is 6x6 km<sup>2</sup>. The annual and national budgets from EMEP/CEIP are disaggregated in space based on proxies of the different sectors of activity (Kuenen et al., 2022). The temporal disaggregation is based  
110 on temporal profiles provided per GNFR sector code with typical month to month, weekday to week-end and diurnal (at 1-hour scale) variations. The TNO-GHGco-v3 inventory is aggregated at the 0.5°x0.5° horizontal resolution of the CHIMERE grid. The resulting prior anthropogenic CO emissions are illustrated in Figure 2a: CO emissions are high over large cities and over industrial areas (e.g. over the Benelux, the Po Valley in Italy, northwestern Germany, southern Poland).

115 In addition to CO, the chemical scheme MELCHIOR-2 needs emissions from other species, such as NMVOCs or nitrogen oxides (NO<sub>x</sub>=NO+NO<sub>2</sub>). Anthropogenic NO<sub>x</sub> emissions are from the TNO-GHGco-v3 inventory while NMVOC anthropogenic emissions are from the EMEP inventory (Vestreng et al., 2005). Biogenic NO<sub>x</sub> and NMVOC emissions, in particular emissions of isoprene and some other hydrocarbons from vegetation, are obtained from the Model of Emissions  
120 of Gases and Aerosols from Nature (MEGAN) model (Guenther et al., 2006).

The resulting monthly means of simulated CO concentrations are illustrated in Figure 3b for CO average surface concentrations in January 2015. The sensitivity of CO simulated concentrations to CO emissions is evaluated by running a sensitivity test with European CO anthropogenic emissions set to zero: the simulated concentrations are illustrated in Figure 4.

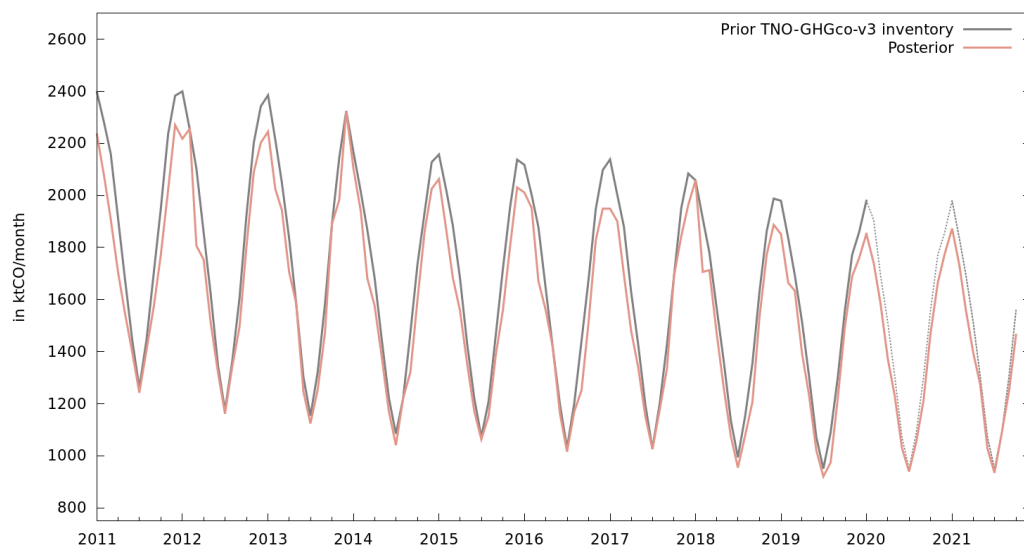


**Figure 1.** Estimates of the monthly budgets of CO for European Union + United Kingdom (EU-27+UK) from the TNO-GHGco-v3 inventory (solid light grey line) and its extension to 2020-2021 (dashed light grey line), and from the regional inversions (solid orange line), from January 2011 to December 2021.

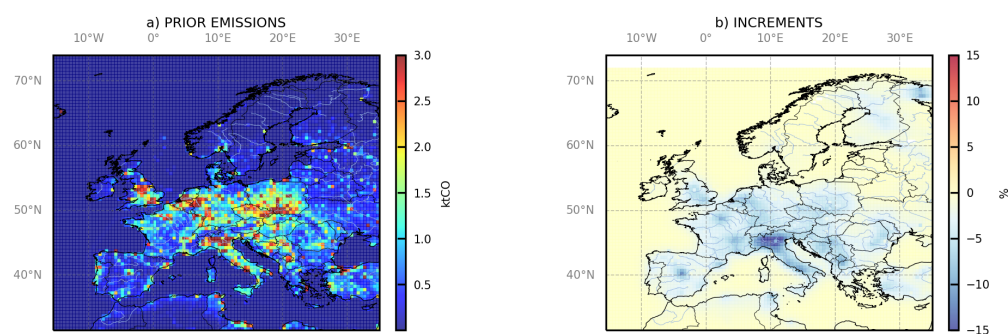


**Figure 2.** a) Monthly CO emissions in ktCO, and b) monthly mean relative increments to the TNO-GHGco-v3 inventory of CO anthropogenic emissions from the inversion in %, in January 2015, at the  $0.5^\circ \times 0.5^\circ$  model resolution.

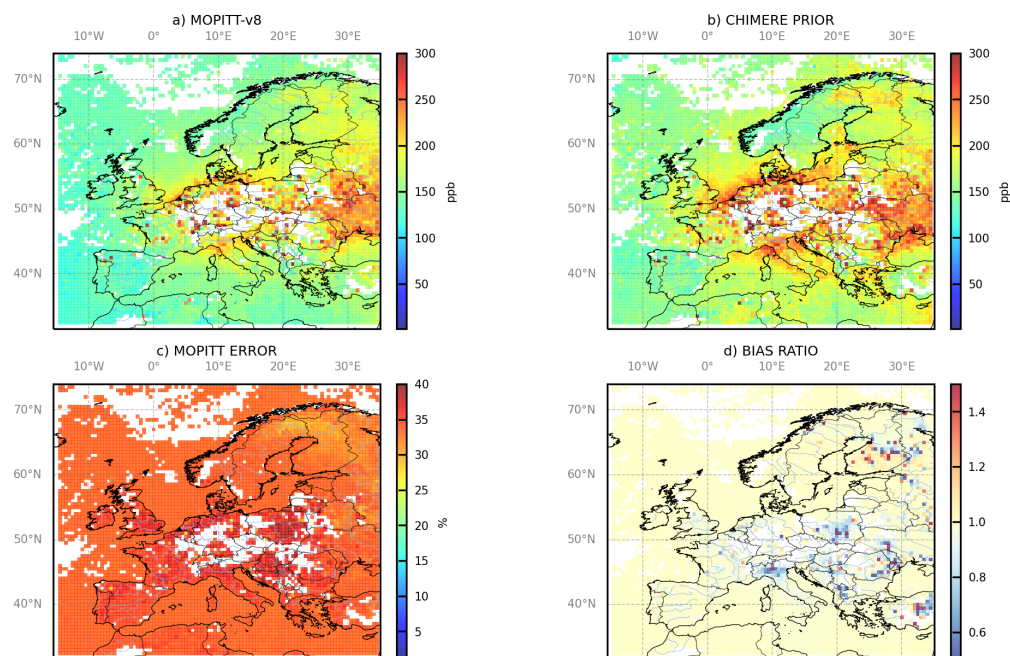


**Figure 3.** Averages of the CO concentrations a) corresponding to the MOPITT "surface super observations" in the CHIMERE grid : a) from MOPITT and b) simulated by CHIMERE using the prior TNO-GHGco-v3 anthropogenic emission estimate, in ppbv. c) Averages of the errors associated with the CO MOPITT super observations, in %. d) Ratios of the posterior and prior biases between monthly mean surface concentrations from CHIMERE and the MOPITT super-observations, at the  $0.5^{\circ} \times 0.5^{\circ}$  grid-cell resolution, in January 2015. All ratios lower than 1, in blue, demonstrate that posterior emission estimates improve the simulation compared to the prior ones.



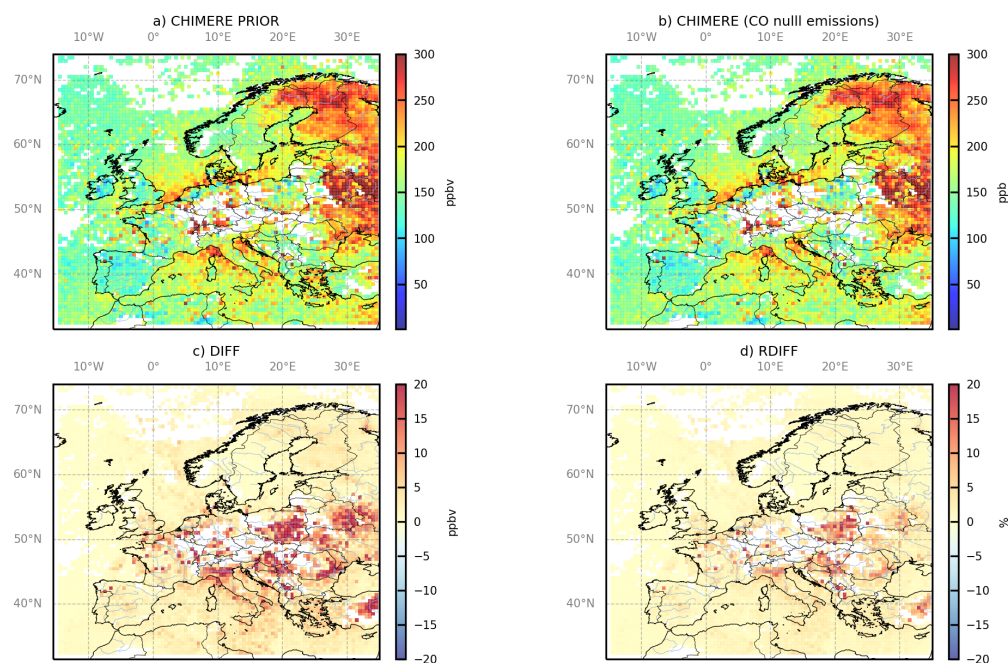


**Figure 4.** Averages of CO concentrations (ppb) a) simulated, using the prior TNO-GHGco-v3 anthropogenic emission estimate, where and when MOPITT-v8J “surface” super observations are available, and b) simulated with null CO emissions. c) Absolute differences a-b (ppb) and d) relative differences  $((a-b)/a)$  (%) between the two simulations.

## 125 2.2 MOPITT satellite observations

CO inversions assimilate CO observations from the MOPITT instrument version 8 (Deeter et al., 2019). MOPITT flies onboard the NASA EOS-Terra satellite, on a low sun-synchronous orbit that crosses the Equator at 10:30 and 22:30 local solar time (LST). The spatial resolution of its observations is about  $22 \times 22$  km<sup>2</sup> at nadir. It has been operated nearly continuously since March 2000.

130 MOPITT CO products are available in three variants: thermal-infrared TIR only, near-infrared NIR only and the multispectral TIR-NIR product, all containing total columns and retrieved profiles (given on a 10-level grid from the surface to 100 hPa). We choose to assimilate the MOPITT “surface” product. Among the different MOPITTv8 products, we choose to work with the multispectral MOPITTv8-NIR-TIR one (also called MOPITT-v8J), as the sensitivity to CO in the



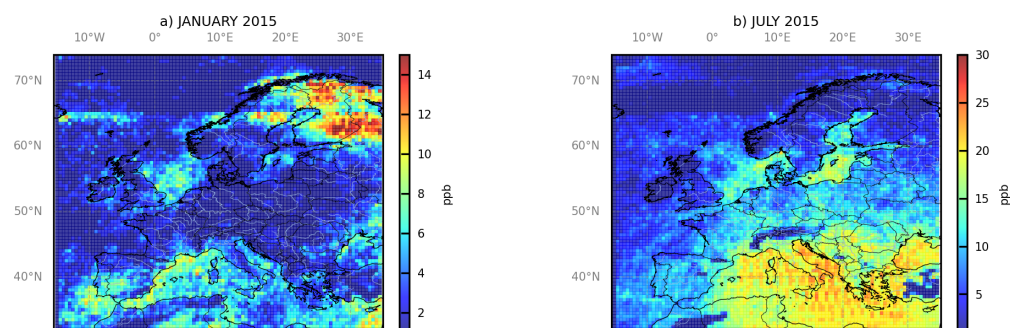


**Figure 5.** Number of MOPITT super-observations in a) January and b) July 2015. Note that the color scales are not the same in both maps.

135 lower troposphere should be significantly greater for retrievals exploiting simultaneous TIR and  
NIR measurements than for retrievals based on either spectral region alone (Deeter et al., 2013).  
In addition, it provides the highest number of data, with a good evaluation against in situ data from  
NOAA stations (Deeter et al., 2019). The MOPITTv8-NIR-TIR surface concentrations are sub-  
sampled within each model grid cell and time-step of the model into single “super-observations”.  
140 In order to associate the super-observations to actual vertical profiles of AK, we selected the me-  
dian of each subset of MOPITT data within each  $0.5^\circ \times 0.5^\circ$  grid cell and each physical time-step  
(about 5-10 min). It is important to note that the potential of MOPITT to provide information can  
be strongly hampered by the cloud coverage in autumn and in winter, as illustrated in Figure 3a  
with blanks for a large part of Central Europe in January 2015. Generally, because of the cloud  
145 cover, the number of MOPITT super-observations is higher in the south of Europe than in Central  
or Northern Europe (Figure 5).

### 2.3 Variational inversion of CO anthropogenic emissions

The inversion of CO emissions consist in correcting the "prior" estimate of these emissions and  
of the model initial and/or boundary conditions to improve the fit between the simulated concen-  
trations and the satellite CO data. The parameters of the variational inversions here closely follow  
the configuration of Fortems-Cheiney et al. (2021), which provides details on on the principle  
and configuration for such inversions. The optimal ("posterior") estimate of the emissions in a



statistical sense is found by iteratively minimizing the following cost function  $J(\mathbf{x})$ :

$$J(\mathbf{x}) = \frac{1}{2}(\mathbf{x} - \mathbf{x}^b)^T \mathbf{B}^{-1}(\mathbf{x} - \mathbf{x}^b) + \frac{1}{2}(\mathcal{H}(\mathbf{x}) - \mathbf{y})^T \mathbf{R}^{-1}(\mathcal{H}(\mathbf{x}) - \mathbf{y})$$

where  $\mathbf{x}$ ,  $\mathcal{H}$ ,  $\mathbf{y}$ ,  $\mathbf{B}$ ,  $\mathbf{R}$  are respectively the control vector, the observation operator, the observations, and covariance matrices as detailed in the following paragraphs.

150 Series of 1-month inversion windows are run. Due to the relatively long lifetime of CO (i.e., few weeks to 2 months Prather (1996)) compared to the size of the studied domain, we account for the CO lateral boundary conditions at the borders of the domain and for their uncertainties.

Therefore, the control vector  $\mathbf{x}$  contains:

- CO anthropogenic emissions at a 1-day temporal resolution, at a  $0.5^\circ \times 0.5^\circ$  resolution and  
155 over the first 8 vertical levels of CHIMERE, i.e., for a one-month inversion, for each of the corresponding (28 to 31 days)  $\times 101 \times 85 \times 8$  grid cells,
- CO lateral boundary conditions at a 1-day temporal resolution, at a  $0.5^\circ \times 0.5^\circ$  resolution and over the 17 vertical levels of CHIMERE, i.e. for each of the corresponding (28 to 31 days)  $\times 372 \times 17$  grid cells,
- 160 – CO 3D initial conditions at 00:00 UTC the first day of the month, at a  $0.5^\circ \times 0.5^\circ$  resolution and over the 17 vertical levels of CHIMERE, i.e. for each of the corresponding  $101 \times 85 \times 17$  grid cells.

It should be noted that the VOCs emissions are fixed and not controlled here by the inversion. Nevertheless, the chemical production of CO by VOCs could be changed due to the correction of  
165 CO boundary conditions and fluxes through chemistry.

$\mathcal{H}$  is the observation operator, which links the control variables to the observed concentrations; it includes the CTM, space and time sampling and other operations (e.g averaging) required to compute the simulated equivalent of the assimilated data. The uncertainties in the observations  $\mathbf{y}$  together with that in the observation operator  $\mathcal{H}$ , and the uncertainties in the prior estimate of the  
170 control vector  $\mathbf{x}^b$  are assumed to have a Gaussian distribution and are thus characterized by their covariance matrices  $\mathbf{R}$  and  $\mathbf{B}$ , respectively. The assumptions and practical way to define these matrices have been detailed by Fortems-Cheiney et al. (2021). The ratios between the prior error standard deviations in  $\mathbf{B}$  and the prior estimates are assigned to 100% for the CO emissions. The ratios between the prior error standard deviations in  $\mathbf{B}$  and the prior estimates are set at 50% for the



175 CO lateral conditions. Spatial correlations are built with exponentially decaying functions with  
an e-folding length of 50 km on land and on sea. Here, the covariance matrix  $\mathbf{R}$  only takes into  
account the estimates of measurement errors reported in the MOPITT data sets. Indeed, the errors  
associated to the observation operators (in particular those associated to the chemistry-transport  
modelling with the CHIMERE configuration for Europe) are ignored since they are assumed to  
180 be much smaller than those associated to the MOPITT data. The minimum of the cost function  $J$   
is searched for with the iterative limited-memory quasi-Newton minimization algorithm MIQN3  
algorithm (Gilbert and Lemaréchal, 1989). At each iteration, the computation of the gradient of  
 $J$  relies on the adjoint of the observation operator, and in particular on the adjoint of CHIMERE.  
In the results presented in Section 3, the norm of the gradient of the cost function  $J$  is reduced by  
185 more than 90%, which indicates robust mathematic behaviour of the system.

The calculation of the uncertainty in the estimate of emissions from the inversion, known as  
“posterior uncertainty”, is challenging when using a variational inverse system (Rayner et al.,  
2019): it is not done here.

### 3 Results

#### 190 3.1 Comparison between simulated and assimilated CO concentrations

The MOPITT data and their prior simulated equivalents present similar spatial patterns for CO  
concentrations, with lowest values over Spain (i.e., with about 125 ppbv) and values higher than  
200 ppbv over Central Europe (over the Benelux, the Po Valley in Italy, northwestern Germany,  
southern Poland, Figure 3). However, the prior simulation overestimates CO concentrations com-  
195 pared to the MOPITT super-observations, in particular over urban and industrial areas in central  
Europe, where the anthropogenic emissions are large (Figure 2a).

By design, the inversions bring the simulated CO concentrations closer to the MOPITT “sur-  
face” super-observations. The corrections made to the prior TNO-GHGco-v3 inventory are par-  
ticularly large in areas where both CO emissions and the sensitivity of CO concentrations to the  
200 emissions are high (Figure 3c, Figure 4). For example, the posterior emissions reduce the mean  
bias between simulated concentrations and MOPITT data by about 26% over the Po Valley in  
Italy and over Benelux in January 2015 (Figure 3c).



Nevertheless, it is worth stressing that the posterior simulation still presents positive biases compared to the observations (Figure 3d). This can be explained by i) large errors in the MOPITT observations that could reach 40% (Figure 3c) and ii) by the relatively weak sensitivity of the simulated concentrations to the local/regional emissions, as illustrated in Figure 4.

### 3.2 Posterior CO emissions

This section focuses on the emissions from the 11-year CO inversion for the period 2011 to 2021. As the prior simulation overestimates CO concentrations compared to the MOPITT super-observations, the inversion applies negative increments to the prior emission estimates (Figure 2). These negative increments mainly occur in fall and winter, even though there is a lower number of observations during these seasons compared to the spring and summer. The highest increments are found over large cities and over industrial areas (Figure 1c). This shows the potential of MOPITT data to provide some information over areas with strong anthropogenic CO emissions

The differences between the prior and posterior CO annual budgets for 30 European countries are shown in Table 3 for the year 2015. Annual budgets of the national emissions are decreased by about 1-11% (Table 3). Similarly, the national and annual increments from 2011 to 2021 range between -1%-11%. Overall, the posterior emission estimates are about 6.3% lower than the prior emissions for the European Union + United Kingdom (EU-27+UK) area in 2015. This indicates that the European CO emissions could be slightly overestimated in the TNO-GHGco-v3 inventory.

The 2011-2021 inversion makes it possible to evaluate the trends and compare them to the ones indicated by the inventories over the decade. As our prior estimates of the emissions for 2020 and 2021 are set at the values for 2019 (see Section 2), trends of CO emissions are only computed from 2011 to 2019. This restriction avoids including the COVID-19 pandemic years.

The TNO-GHGco-v3 CO emissions show a decreasing trend over EU-27+UK area from 2011 to 2019 (Figure 1), of about -2.5%/year ( $p=9.5 \times 10^{-4}$ ). These decreasing trends are mainly driven by the transport sector (Zheng et al., 2019) with progressive pollution control on vehicles that has cut down CO European emissions (Crippa et al., 2016). Interestingly, the trends from 2011 to 2019 in the TNO inventory, based on the EMEP official reporting, exhibit some disparities depending on the countries with for example, a stronger decreasing trend over France than over Germany.

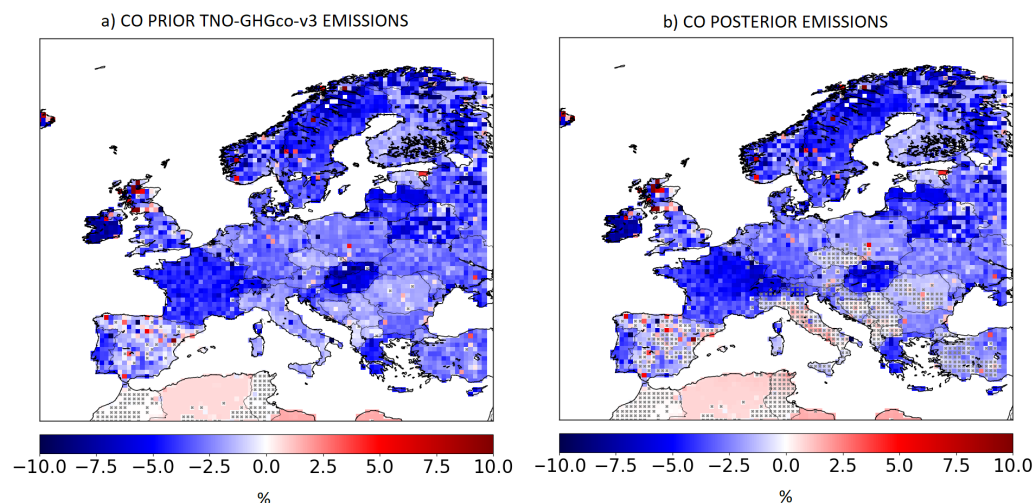


**Figure 6.** Trends of CO emissions from 2011 to 2019 (a) in the TNO-GHGco-v3 inventory and b) in the posterior emissions, in %/yr. Crosses show pixels with insignificant trend ( $p$ -value higher than 0.05).

The posterior CO emissions display a very similar decreasing trend than the prior emissions over the EU-27+UK area (Figure 1) of about -2.2 %/year ( $p=2.2 \times 10^{-3}$ ). The main differences between the prior and posterior trends are found for the autumn and winter months, with a posterior trend of about -1.9%/year compared to the prior trend of about -2.4%/year. Spatially, the differences are larger in Italy, in Czech Republic and in the Balkans than in the rest of Europe (Figure 6). While the TNO-GHGco-v3 inventory shows significant decreasing trends in these regions, the posterior emissions are steadily increasing. These areas benefit from the best MOPITT coverage, with the highest number of MOPITT super-observations (Figure 5). Consequently, the assimilation of MOPITT observations in the inversions attenuate the strong decreasing trend of the CO emissions in the TNO-GHGco-v3 inventory, particularly during autumn and winter.

Finally, there is no significant inter-annual variability from 2011 to 2019, neither in the prior nor in the posterior CO emissions. A particular attention has consequently been put on the possible detection of an inter-annual anomaly linked to the policies implemented in response to the COVID-19 in 2020.



### 3.3 Impact of COVID-19

Following a usual diagnostic in the literature to assess the change in air pollutants concentrations due to the COVID-19 policies, we characterize the impact of the COVID-19 policies in terms of change of emissions budgets from April 2019 to April 2020. Most of the European countries implemented lock-down policies in April, after a progressive implementation of the national lock-downs from 9 March 2020 (Italy) to 23 March 2020 (United Kingdom, UK). The change from April 2019 to April 2020 potentially includes variations associated to drivers of the usual emission processes (e.g. changes of temperature from 2019 to 2020) but as indicated above, the typical inter-annual variations in both the prior and posterior estimates are relatively small. Since the prior estimates for 2020 and 2019 are identical (see Section 2), we actually analyze the impact of the COVID-19 policies in terms of differences of increments provided by the inversions to these prior estimates between April 2019 and April 2020. Overall a much smaller lock-down-driven impact is expected for CO than for NO<sub>2</sub>, particularly because of smaller contributions from lock-down-affected sources (Clark et al., 2021).

At the European scale, the CO posterior emission estimates derived from the MOPITT data decrease by about -1.3% in April 2020 compared to April 2019. This decrease is lower than the estimates of about -4.7%, -6.4%, -7.6% and -8.2% of, respectively, Guevara et al. (2023), Doumbia et al. (2021), Forster et al. (2021) and from the officially reported emissions from EMEP/CEIP (CEIP, 2022).

Nevertheless, as shown in Figure 7, the inversions lead to a higher decrease of CO emissions over the areas where the anthropogenic emissions are usually large, and particularly over industrial basins such as over the Benelux/Rhine-Rhur Valley where the decrease reaches -8% and over the Po Valley where it reaches -10% in April 2020 compared to April 2019 (Figure 7c).

## 270 4 Discussion and Conclusion

The CIF, coupled to the regional chemistry-transport model CHIMERE and its adjoint, and the satellite CO MOPITT data have been used to estimate 11 years from 2011 to 2021 of European CO emissions. The analysis of the inversion results reveal the challenges associated with the inversion of CO emissions at the regional scale over Europe. Annual budgets of the national emissions are



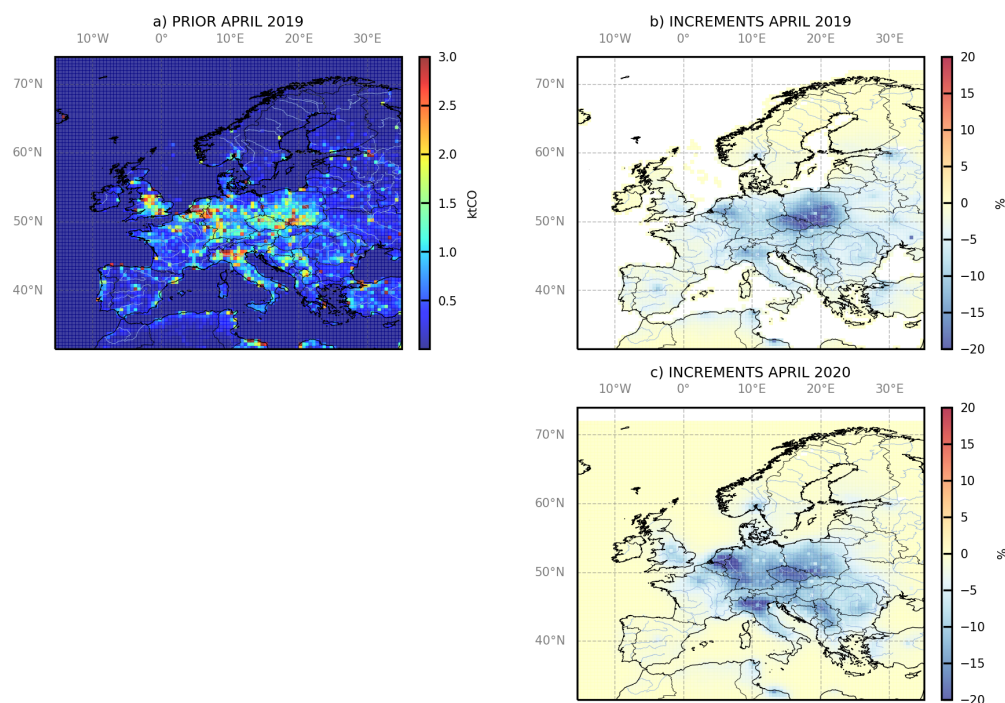


**Figure 7.** a) Emissions estimated by the TNO inventory in April 2019, in ktCO/month. Increment provided by the inversions in b) April 2019 and c) April 2020, in %.

275 decreased by about 1-11% over the decade and over Europe. These decreases are mainly due to  
negative corrections during autumn and winter.

280 The posterior CO emissions display a very similar decreasing trend than the prior emissions  
over the EU-27+UK area with a trend of about -2.2 %/year, showing a general consistency with  
reported anthropogenic emissions. This trend is slightly lower than in the prior emissions. The  
assimilation of the MOPITT observation in the inversions indeed attenuate the decreasing trend  
of the CO emissions in the TNO inventory over areas benefiting from the highest number of  
MOPITT super-observations (particularly over Italy and over the Balkans), and particularly in  
autumn and winter.

285 The posterior simulation still presents positive biases compared to the observations, which  
can be partly explained by large errors in the MOPITT observations. Also, a refinement of the



inversion strategy may support a better fit to the observations. In particular, under the assumptions that uncertainties in the control variables have a Gaussian distribution, the control of the logarithm of the emissions rather than of scaling factor for these emissions may better correspond to our CO inversion problem, in which CO emissions are necessarily positive, but in which these emissions could have to be strongly decreased. Opposed to the Gaussian characterization and to the spatial correlation of the uncertainties in the emissions, the Gaussian characterization and the spatial correlation of the uncertainties in logarithm of the emissions could increase the flexibility for large local corrections of the emissions. The current characterization of the uncertainties in the CO emissions using a Gaussian distribution may actually contribute to the limitation of the fit to the observations.

The small corrections of the CO emissions at national scales by the inversion can be attributed, first, to the general consistency between the TNO-GHGco-v3 inventory and the satellite data. However, analysis of specific patterns such as the impact of the covid-19 crisis reveal that it can also be seen as a lack of observation constraint to adjust the prior estimate of the emissions. The large errors in the observations, and the lack of data over large parts of Europe are definitely some sources of limitation on the observational constraint.

However, in a more general way, this questions the ability to exploit large scale variations in the CO satellite data to constrain regional and national to continental scale budgets of the emissions. Emission hot spots generate a relatively strong local signal, which is much better caught and exploited by the inversions than the larger scale signals, despite the moderate spatial resolution of the MOPITT data. This is why the corrections of these hot spot emissions are stronger and more convincing than the corrections of the national and continental scale emissions, as shown by the analysis of the impact of covid-19 policies. Accurate monitoring of the national anthropogenic CO emissions will likely rely more on the aggregation of local emission monitoring data rather than on the processing of large scale variations in the CO fields. The former requires modeling and inversion systems at spatial resolution finer than those used here, as well satellite images at high spatial resolution. The CO images of the TROPOMI instrument onboard the Sentinel-5P mission with a 5.5km x7 km resolution since August 2019 should be well suited for such a perspective. The large increase in the number of observations with this mission is expected to increase the capabilities to monitor CO emissions and to address air-quality-related emissions at the national to subnational scales.



## 5 Open Research

MOPITT version 8 products are freely available through NASA's EarthData portal at <https://earthdata.nasa.gov/>,  
(Deeter et al., 2019). The TNO-GHGco-v3 inventory (Super et al., 2020) is available upon request  
320 from TNO (contact: Hugo Denier van der Gon, [hugo.deniervandergon@tno.nl](mailto:hugo.deniervandergon@tno.nl)). The CHIMERE  
code is available here: [www.lmd.polytechnique.fr/chimere/](http://www.lmd.polytechnique.fr/chimere/), (Menuet et al., 2013; Mailler et al.,  
2017). The CIF inversion system (Berchet et al., 2021) is available at : <http://community-inversion.eu/>

*Acknowledgements.* We acknowledge the NCAR MOPITT group for the production of the CO retrievals.  
A large part of the development and analysis were conducted in the frame of the H2020 VERIFY project,  
325 funded by the European Commission Horizon 2020 research and innovation programme, under agreement  
number 776810. We wish to thank all the persons involved in the preparation, coordination and management  
of this project. This project has also received funding from the French ANR project ARGONAUT under  
grant agreement No ANR-19-CE01-0007 and from the French PRIMEQUAL project LOCKAIR under grant  
agreement No 2162D0010. This work was supported by the CNES (Centre National d'Etudes Spatiales), in  
330 the frame of the TOSCA ARGOS project. This work was granted access to the HPC resources of TGCC  
under the allocations A0100102201 and A0110102201 made by GENCI. Finally, we wish to thank J. Bruna  
(LSCE) and his team for computer support.

The authors declare that they have no conflict of interest.



Country Code	Difference between CO anthropogenic emissions estimates from the inversions and TNO-GHGco-v3 in %
ALB	-5.9
AUT	-8.0
BEL	-6.2
BLR	-0.6
CHE	-8.4
DEU	-7.6
DNK	-1.2
ESP	-4.1
FIN	-0.5
FRA	-5.3
GBR	-3.3
IRL	-0.8
ITA	-11.4
LUX	-6.3
NLD	-6.8
NOR	-1.0
PRT	-3.0
SWE	-0.4
BGR	-4.0
CZE	-10.6
EST	-0.3
HRV	8.94
HUN	-7.1
LTU	-0.7
LVA	-0.4
POL	-6.7
ROU	-5.6
SVN	-9.1
SVK	-7.8
UKR	-3.4
EU-27+UK	-6.3

**Table 2.** Difference between the CO annual emissions from the TNO-GHGco-v3 inventory used as prior in this study and from the inversions, by country, in %, in 2015.



Country Code	Difference between CO posterior emissions estimates in April 2020 and in April 2019 in %
BEL	-5.6
CHE	-3.5
DEU	-7.3
FRA	-1.2
GBR	-0.4
ITA	-3.5
LUX	-5.4
NLD	-7.7
EU-27+UK	-1.3

**Table 3.** Difference between the CO posterior emissions in April 2020 and in April 2019, by country, in %.



## References

- 335 Aumann, H., Chahine, M., Gautier, C., Goldberg, M., Kalnay, E., McMillin, L., Revercomb, H., Rosenkranz, P., Smith, W., Staelin, D., Strow, L., and Susskind, J.: AIRS/AMSU/HSB on the Aqua mission: design, science objectives, data products, and processing systems, *IEEE Transactions on Geoscience and Remote Sensing*, 41, 253–264, <https://doi.org/10.1109/TGRS.2002.808356>, 2003.
- Beer, R.: TES on the aura mission: scientific objectives, measurements, and analysis overview, *IEEE Transactions on Geoscience and Remote Sensing*, 44, 1102–1105, <https://doi.org/10.1109/TGRS.2005.863716>, 2006.
- 340 Berchet, A., Sollum, E., Thompson, R. L., Pison, I., Thanwerdas, J., Broquet, G., Chevallier, F., Aalto, T., Berchet, A., Bergamaschi, P., Brunner, D., Engelen, R., Fortems-Cheiney, A., Gerbig, C., Groot Zwaafink, C. D., Haussaire, J.-M., Henne, S., Houweling, S., Karstens, U., Kutsch, W. L., Lujckx, I. T., Monteil, G., Palmer, P. I., van Peet, J. C. A., Peters, W., Peylin, P., Potier, E., Rödenbeck, C., Saunio, M., Scholze, M., Tsuruta, A., and Zhao, Y.: The Community Inversion Framework v1.0: a unified system for atmospheric inversion studies, *Geoscientific Model Development*, 14, 5331–5354, <https://doi.org/10.5194/gmd-14-5331-2021>, 2021.
- 345 Buchholz, R. R., Worden, H. M., Park, M., Francis, G., Deeter, M. N., Edwards, D. P., Emmons, L. K., Gaubert, B., Gille, J., Martínez-Alonso, S., Tang, W., Kumar, R., Drummond, J. R., Clerbaux, C., George, M., Coheur, P.-F., Hurtmans, D., Bowman, K. W., Luo, M., Payne, V. H., Worden, J. R., Chin, M., Levy, R. C., Warner, J., Wei, Z., and Kulawik, S. S.: Air pollution trends measured from Terra: CO and AOD over industrial, fire-prone, and background regions, *Remote Sensing of Environment*, 256, 112275, <https://doi.org/https://doi.org/10.1016/j.rse.2020.112275>, 2021.
- 350 CEIP: EMEP Centre on Emissions Inventories and Projections, Officially reported emission data, Tech. rep., <https://www.ceip.at/webdab-emission-database/reported-emissiondata>, 2022.
- CHIMERE: Documentation of the chemistry-transport model CHIMERE, Tech. rep., <https://www.lmd.polytechnique.fr/chimere/docs/CHIMEREdoc2017.pdf>, 2017.
- 355 Clark, H., Bennouna, Y., Tsvilidou, M., Wolff, P., Sauvage, B., Barret, B., Le Flochmoën, E., Blot, R., Boulanger, D., Cousin, J.-M., Nédélec, P., Petzold, A., and Thouret, V.: The effects of the COVID-19 lockdowns on the composition of the troposphere as seen by In-service Aircraft for a Global Observing System (IAGOS) at Frankfurt, *Atmospheric Chemistry and Physics*, 21, 16237–16256, <https://doi.org/10.5194/acp-21-16237-2021>, 2021.
- 360 Clerbaux, C., Boynard, A., Clarisse, L., George, M., Hadji-Lazaro, J., Herbin, H., Hurtmans, D., Pommier, M., Razavi, A., Turquety, S., Wespes, C., and Coheur, P.-F.: Monitoring of atmospheric composition using the thermal infrared IASI/MetOp sounder, *Atmospheric Chemistry and Physics*, 9, 6041–6054, <https://doi.org/10.5194/acp-9-6041-2009>, 2009.





- Crippa, M., Janssens-Maenhout, G., Dentener, F., Guizzardi, D., Sindelarova, K., Muntean, M.,  
Van Dingenen, R., and Granier, C.: Forty years of improvements in European air quality: regional  
370 policy-industry interactions with global impacts, *Atmospheric Chemistry and Physics*, 16, 3825–3841,  
<https://doi.org/10.5194/acp-16-3825-2016>, 2016.
- Deeter, M. N., Emmons, L. K., Francis, G. L., Edwards, D. P., Gille, J. C., Warner, J. X., Khat-  
tatov, B., Ziskin, D., Lamarque, J.-F., Ho, S.-P., Yudin, V., Attié, J.-L., Packman, D., Chen,  
J., Mao, D., and Drummond, J. R.: Operational carbon monoxide retrieval algorithm and se-  
375 lected results for the MOPITT instrument, *Journal of Geophysical Research: Atmospheres*, 108,  
<https://doi.org/https://doi.org/10.1029/2002JD003186>, 2003.
- Deeter, M. N., Martínez-Alonso, S., Edwards, D. P., Emmons, L. K., Gille, J. C., Worden, H. M., Pittman,  
J. V., Daube, B. C., and Wofsy, S. C.: Validation of MOPITT Version 5 thermal-infrared, near-infrared,  
and multispectral carbon monoxide profile retrievals for 2000–2011, *Journal of Geophysical Research:*  
380 *Atmospheres*, 118, 6710–6725, <https://doi.org/https://doi.org/10.1002/jgrd.50272>, 2013.
- Deeter, M. N., Edwards, D. P., Francis, G. L., Gille, J. C., Mao, D., Martínez-Alonso, S., Worden, H. M.,  
Ziskin, D., and Andreae, M. O.: Radiance-based retrieval bias mitigation for the MOPITT instrument: the  
version 8 product, *Atmospheric Measurement Techniques*, 12, 4561–4580, <https://doi.org/10.5194/amt-12-4561-2019>, 2019.
- 385 Denier van der Gon, H., Dellaert, S., I. Super, J. K., and Visschedijk, A.: Final High Resolution emission  
data 2005–2018, Tech. rep., [https://verify.lscce.ipsl.fr/images/PublicDeliverables/VERIFY\\_D2\\_3\\_TNO\\_](https://verify.lscce.ipsl.fr/images/PublicDeliverables/VERIFY_D2_3_TNO_v1.pdf)  
[v1.pdf](https://verify.lscce.ipsl.fr/images/PublicDeliverables/VERIFY_D2_3_TNO_v1.pdf), 2021.
- Doumbia, T., Granier, C., Elguindi, N., Bouarar, I., Darras, S., Brasseur, G., Gaubert, B., Liu, Y., Shi, X.,  
Stavrou, T., Tilmes, S., Lacey, F., Deroubaix, A., and Wang, T.: Changes in global air pollutant emis-  
390 sions during the COVID-19 pandemic: a dataset for atmospheric modeling, *Earth System Science Data*,  
13, 4191–4206, <https://doi.org/10.5194/essd-13-4191-2021>, 2021.
- Drummond, J. R., Mand, G., and Bailak, G. V.: Calibration of the MOPITT instrument for EOS, in: *Optics*  
*+ Photonics*, 1996.
- Forster, P., Forster, H., and Evans, M. e. a.: Current and future global climate impacts resulting from COVID-  
395 19, *Nat. Clim. Chang.*, 10, 913–919, <https://doi.org/10.1038/s41558-020-0883-0>, 2021.
- Fortems-Cheiney, A., Chevallier, F., Pison, I., Bousquet, P., Szopa, S., Deeter, M. N., and Clerbaux, C.: Ten  
years of CO emissions as seen from Measurements of Pollution in the Troposphere (MOPITT), *Journal of*  
*Geophysical Research: Atmospheres*, 116, <https://doi.org/https://doi.org/10.1029/2010JD014416>, 2011.
- Fortems-Cheiney, A., Pison, I., Broquet, G., Dufour, G., Berchet, A., Potier, E., Coman, A., Siour, G.,  
400 and Costantino, L.: Variational regional inverse modeling of reactive species emissions with PYVAR-



- CHIMERE-v2019, *Geoscientific Model Development*, 14, 2939–2957, <https://doi.org/10.5194/gmd-14-2939-2021>, 2021.
- George, M., Clerbaux, C., Bouarar, I., Coheur, P.-F., Deeter, M. N., Edwards, D. P., Francis, G., Gille, J. C., Hadji-Lazaro, J., Hurtmans, D., Inness, A., Mao, D., and Worden, H. M.: An examination of the long-term  
405 CO records from MOPITT and IASI: comparison of retrieval methodology, *Atmospheric Measurement Techniques*, 8, 4313–4328, <https://doi.org/10.5194/amt-8-4313-2015>, 2015.
- Gilbert, J. and Lemaréchal, C.: Some numerical experiments with variable storage quasi Newton algorithms, *Math. Program.*, 45, 407–435, <https://doi.org/10.1007/BF01589113>, 1989.
- Guenther, A., Karl, T., Harley, P., Wiedinmyer, C., Palmer, P. I., and Geron, C.: Estimates of global terrestrial isoprene emissions using MEGAN (Model of Emissions of Gases and Aerosols from Nature), *Atmospheric Chemistry and Physics*, 6, 3181–3210, <https://doi.org/10.5194/acp-6-3181-2006>, 2006.
- Guevara, M., Petetin, H., Jorba, O., Denier van der Gon, H., Kuenen, J., Super, I., Granier, C., Doumbia, T., Ciais, P., Liu, Z., Lamboll, R. D., Schindlbacher, S., Matthews, B., and Pérez García-Pando, C.: Towards  
415 near-real time air pollutant and greenhouse gas emissions: lessons learned from multiple estimates during the COVID-19 Pandemic, *EGUsphere*, 2023, 1–36, <https://doi.org/10.5194/egusphere-2023-186>, 2023.
- Konovalov, I. B., Berezin, E. V., Ciais, P., Broquet, G., Zhuravlev, R. V., and Janssens-Maenhout, G.: Estimation of fossil-fuel CO<sub>2</sub> emissions using satellite measurements of “proxy” species, *Atmospheric Chemistry and Physics*, 16, 13 509–13 540, <https://doi.org/10.5194/acp-16-13509-2016>, 2016.
- 420 Kuenen, J. and Dore, C.: EMEP/EEA air pollutant emission inventory guidebook 2019: Uncertainties, Tech. rep., <https://www.eea.europa.eu/publications/emep-eea-guidebook-2019/part-a-general-guidance-chapters/5-uncertainties>, 2019.
- Kuenen, J., Dellaert, S., Visschedijk, A., Jalkanen, J.-P., Super, I., and Denier van der Gon, H.: CAMS-REG-v4: a state-of-the-art high-resolution European emission inventory for air quality modelling, *Earth System  
425 Science Data*, 14, 491–515, <https://doi.org/10.5194/essd-14-491-2022>, 2022.
- Lelieveld, J., Gromov, S., Pozzer, A., and Taraborrelli, D.: Global tropospheric hydroxyl distribution, budget and reactivity, *Atmospheric Chemistry and Physics*, 16, 12 477–12 493, <https://doi.org/10.5194/acp-16-12477-2016>, 2016.
- Mailler, S., Menut, L., Khvorostyanov, D., Valari, M., Couvidat, F., Siour, G., Turquety, S., Briant, R.,  
430 Tuccella, P., Bessagnet, B., Colette, A., Létinois, L., Markakis, K., and Meleux, F.: CHIMERE-2017: from urban to hemispheric chemistry-transport modeling, *Geoscientific Model Development*, 10, 2397–2423, <https://doi.org/10.5194/gmd-10-2397-2017>, 2017.
- McMillan, W. W., Barnet, C., Strow, L., Chahine, M. T., McCourt, M. L., Warner, J. X., Novelli, P. C., Korontzi, S., Maddy, E. S., and Datta, S.: Daily global maps of car-



- 435 bon monoxide from NASA's Atmospheric Infrared Sounder, *Geophysical Research Letters*, 32,  
<https://doi.org/https://doi.org/10.1029/2004GL021821>, 2005.
- Menut, L., Bessagnet, B., Khvorostyanov, D., Beekmann, M., Blond, N., Colette, A., Coll, I., Curci, G.,  
Foret, G., Hodzic, A., Mailler, S., Meleux, F., Monge, J.-L., Pison, I., Siour, G., Turquety, S., Valari, M.,  
Vautard, R., and Vivanco, M. G.: CHIMERE 2013: a model for regional atmospheric composition mod-  
440 elling, *Geoscientific Model Development*, 6, 981–1028, <https://doi.org/10.5194/gmd-6-981-2013>, 2013.
- Owens, R. G. and Hewson, T.: ECMWF Forecast User Guide, Tech. rep.,  
<https://doi.org/https://doi.org/10.21957/m1cs7h>, 2018.
- Prather, M. J.: Time scales in atmospheric chemistry: Theory, GWPs for CH<sub>4</sub> and CO, and runaway growth,  
*Geophysical Research Letters*, 23, 2597–2600, <https://doi.org/https://doi.org/10.1029/96GL02371>, 1996.
- 445 Rayner, P. J., Michalak, A. M., and Chevallier, F.: Fundamentals of data assimilation applied to bio-  
geochemistry, *Atmospheric Chemistry and Physics*, 19, 13 911–13 932, <https://doi.org/10.5194/acp-19-13911-2019>, 2019.
- San-Miguel-Ayanz, J. and Steinbrecher, R.: EMEP/EEA air pollutant emission inventory guide-  
book 2019: Forest and other vegetation fires, Tech. rep., [https://www.eea.europa.eu/publications/  
450 emep-eea-guidebook-2019/part-b-sectoral-guidance-chapters/11-natural-sources/11-b-forest-fires/  
view](https://www.eea.europa.eu/publications/emep-eea-guidebook-2019/part-b-sectoral-guidance-chapters/11-natural-sources/11-b-forest-fires/view), 2019.
- Super, I., Dellaert, S. N. C., Visschedijk, A. J. H., and Denier van der Gon, H. A. C.: Uncertainty analysis of  
a European high-resolution emission inventory of CO<sub>2</sub> and CO to support inverse modelling and network  
design, *Atmospheric Chemistry and Physics*, 20, 1795–1816, <https://doi.org/10.5194/acp-20-1795-2020>,  
455 2020.
- Szopa, S. and Foret, G. M. L. C. A.: Impact of large scale circulation on European  
summer surface ozone: consequences for modeling, *Atmospheric Environment*, 43,  
<https://doi.org/doi:10.1016/j.atmosenv.2008.10.0390>, 2008.
- Vestreng, V., Breivik, K. and Adams, M., Wagner, A., Goodwin, J., Rozovskaya, O., and Oacyna, J.: Inven-  
460 tory Review 2005 - Emission Data reported to CLRTAP and under the NEC Direc-tive - Initial review for  
HMs and POPs, Tech. rep., 2005.
- Yin, Y., Chevallier, F., Ciais, P., Broquet, G., Fortems-Cheiney, A., Pison, I., and Saunois, M.: Decadal trends  
in global CO emissions as seen by MOPITT, *Atmospheric Chemistry and Physics*, 15, 13 433–13 451,  
<https://doi.org/10.5194/acp-15-13433-2015>, 2015.
- 465 Zheng, B., Chevallier, F., Ciais, P., Yin, Y., Deeter, M. N., Worden, H. M., Wang, Y., Zhang, Q., and He, K.:  
Rapid decline in carbon monoxide emissions and export from East Asia between years 2005 and 2016,  
*Environmental Research Letters*, 13, 044 007, <https://doi.org/10.1088/1748-9326/aab2b3>, 2018.

<https://doi.org/10.5194/egusphere-2023-1981>

Preprint. Discussion started: 6 October 2023

© Author(s) 2023. CC BY 4.0 License.



470 Zheng, B., Chevallier, F., Yin, Y., Ciais, P., Fortems-Cheiney, A., Deeter, M. N., Parker, R. J., Wang, Y., Worden, H. M., and Zhao, Y.: Global atmospheric carbon monoxide budget 2000–2017 inferred from multi-species atmospheric inversions, *Earth System Science Data*, 11, 1411–1436, <https://doi.org/10.5194/essd-11-1411-2019>, 2019.